


# ATRX status in patients with gliomas

## Radiomics analysis

Linlin Meng, MD<sup>a</sup>, Ran Zhang, MD<sup>b</sup>, Liangguo Fa, PhD<sup>a</sup>, Lulu Zhang, MD<sup>c</sup>, Linlin Wang, MD<sup>a</sup>, Guangrui Shao, PhD<sup>a,\*</sup> 

### Abstract

The aim of this study was to develop a noninvasive radiomics analysis model based on preoperative multiparameter MRI to predict the status of the biomarker alpha thalassemia/mental retardation X-linked syndrome (ATRX) in glioma noninvasively.

**Material and methods:** A cohort of 123 patients diagnosed with gliomas (World Health Organization grades II–IV) who underwent surgery and was treated at our center between January 2016 and July 2020, was enrolled in this retrospective study. Radiomics features were extracted from MR T1WI, T2WI, T2FLAIR, CE-T1WI, and ADC images. Patients were randomly split into training and validation sets at a ratio of 4:1. A radiomics signature was constructed using the least absolute shrinkage and selection operator (LASSO) to train the SVM model using the training set. The prediction accuracy and area under curve and other evaluation indexes were used to explore the performance of the model established in this study for predicting the ATRX mutation state.

**Results:** Fifteen radiomic features were selected to generate an ATRX-associated radiomic signature using the LASSO logistic regression model. The area under curve for ATRX mutation (ATRX(–)) on training set was 0.93 (95% confidence interval [CI]: 0.87–1.0), with the sensitivity, specificity and accuracy being 0.91, 0.82 and 0.88, while on the validation set were 0.84 (95% CI: 0.63–0.91), with the sensitivity, specificity and accuracy of 0.73, 0.86, and 0.79, respectively.

**Conclusions:** These results indicate that radiomic features derived from preoperative MRI facilitate efficient prediction of ATRX status in gliomas, thus providing a novel evaluation method for noninvasive imaging biomarkers.

**Abbreviations:** ADC = apparent diffusion coefficient, ALT = alternative lengthening of telomeres, ATRX = alpha thalassemia/mental retardation X-linked syndrome, AUC = Area under curve, CE = contrast enhanced, DWI = diffusion weighted imaging, FOV = field of view, GLDM = gray-level dependence matrix, GLSZM = gray-level size zone matrix, ICC = intraclass correlation coefficient, IDH = isocitrate dehydrogenase, LASSO = least absolute shrinkage and selection operator, MRI = magnetic resonance imaging, mRMR = minimum redundancy maximum relevance, NEX = number of excitations, RBF = radial basis function, ROC = receiver operating characteristic, SVM = support vector machine, TE = echo time, TI = inversion time, TR = repetition time, VEGF = vascular endothelial growth factor, VOI = volume of interest.

**Keywords:** alpha thalassemia/mental retardation X-linked syndrome, glioma, magnetic resonance imaging, radiomics

## 1. Introduction

Gliomas are the most common primary malignant brain tumors,<sup>[1]</sup> ranging from benign to malignant tumors, with a diverse array of genomic differences and clinical outcomes. So far, conventional magnetic resonance imaging (MRI) has been used as an indispensable method for noninvasive diagnosis and prognosis evaluation of glioma. With the development of precision medicine, the molecular testing of gliomas has become an important part which can help us to better understand the biological properties of this malignancy, improve the diagnostic

level, and guide clinical decision making.<sup>[2–5]</sup> In 2016, the World Health Organization used molecular diagnosis as a new classification criteria for tumors of the central nervous system and introduced the alpha thalassemia/mental retardation X-linked syndrome (ATRX) mutation to explore the diagnostic significance of mutant/wild-type isocitrate dehydrogenase 1 (IDH1) for glioma classification,<sup>[6–8]</sup> ushering a new era of differentiation and treatment of brain tumors.

ATRX is located on the Xq21.1 chromosome and encodes a 280 kDa nucleoprotein, which is involved in numerous cellular functions, including DNA recombination, repair, advanced

The authors have no funding and conflicts of interest to disclose.

The datasets generated during and/or analyzed during the current study are available from the corresponding author on reasonable request. All data generated or analyzed during this study are included in this published article (and its supplementary information files).

This study was approved and reviewed by the institutional review board of the institution (The Second Hospital, Cheeloo College of Medicine, Shandong University). The requirement for informed consent was waived.

<sup>a</sup>Department of Radiology, The Second Hospital, Cheeloo College of Medicine, Shandong University, Jinan, Shandong, China, <sup>b</sup>Huiying Medical Technology Co. Ltd, Beijing, China, <sup>c</sup>Department of Pathology, The Second Hospital, Cheeloo College of Medicine, Shandong University, Jinan, Shandong, China.

\* Correspondence: Guangrui Shao, Department of Radiology, The Second Hospital, Cheeloo College of Medicine, Shandong University, No. 247 Beiyuan Road, Jinan, Shandong (e-mail: shaoguangrui123@126.com).

Copyright © 2022 the Author(s). Published by Wolters Kluwer Health, Inc. This is an open-access article distributed under the terms of the Creative Commons Attribution-Non Commercial License 4.0 (CCBY-NC), where it is permissible to download, share, remix, transform, and build up the work provided it is properly cited. The work cannot be used commercially without permission from the journal.

How to cite this article: Meng L, Zhang R, Fa L, Zhang L, Wang L, Shao G. ATRX status in patients with gliomas: Radiomics analysis. *Medicine* 2022;101:37(e30189).

Received: 17 September 2021 / Received in final form: 14 February 2022 / Accepted: 20 May 2022

<http://dx.doi.org/10.1097/MD.00000000000030189>

chromatin regulation, and gene transcriptional regulation.<sup>[9]</sup> ATRX plays an important role in chromatin modulation and maintenance of telomeres.<sup>[10]</sup> ATRX mutation denotes loss of ATRX expression, interpreted as loss of nuclear staining in the majority of the tumor cells in the presence of an internal positive control.<sup>[11]</sup> Human ATRX mutations are present in at least 15 types of human tumors, including neuroblastoma, osteosarcoma and pancreatic neuroendocrine tumors,<sup>[12]</sup> which can lead to the development of thalassemia, mental retardation,  $\alpha$ -thalassemia X-linked mental retardation and other genetic conditions.<sup>[13]</sup> In adults, ATRX mutations occur in 71% of grade II-III astrocytomas, 68% of oligoastrocytomas, and 57% of secondary glioblastomas.<sup>[14-18]</sup> However, the role of ATRX in gliomas is still in its infancy. So far, studies have found ATRX deletions/mutations were closely associated with IDH mutations<sup>[15,19,20]</sup> and tumor suppressor gene TP53 mutations.<sup>[21-23]</sup> Therefore, the detection of ATRX status is particularly useful for further guiding glioma classification and diagnosis, as well as pointing directions toward individualized treatment of glioma patients.

Currently, the ATRX status can only be detected following surgery or biopsy, both are invasive methods and cannot predict the patient prognosis before surgical resection. On the other hand, owing to the heterogeneity of tumors, different tissue sampling sites may lead to different detection results.

Radiomics is a rapidly expanding research field in medical image analysis that involves handling numerous texture features of radiographic images to construct an objective-driven prediction model.<sup>[23]</sup> Multi-features can comprehensively reflect the intrinsic microscopic pathological characteristics of disease, which then can be used to diagnose or evaluate the prognosis. Their potential application in clinical practice has attracted significant attention in recent years. On the background of the novel coronavirus disease 2019, a combined model consisting of 2-dimensional curvelet transformation, meta-heuristic optimization algorithm and deep learning technique had been proposed to diagnose the patient infected with coronavirus pneumonia from X-ray images.<sup>[24]</sup> Several attempts also have shown the feasibility of radiomics for predicting patient’s molecular markers. Zhang et al<sup>[25]</sup> have used random forest based on clinical variables and multimodal features extracted from conventional MRI to predict IDH genotype in high-grade gliomas. Sun et al<sup>[26]</sup>

have used the minimum redundancy maximum relevance algorithm and support vector machine (SVM) based on preoperative T2-weighted images to predict vascular endothelial growth factor (VEGF) expression in patients with diffuse gliomas. Furthermore, Kickingreder et al<sup>[27]</sup> have used machine learning method to evaluate the association of multiparametric and multi-regional MR imaging features with key molecular characteristics in high-grade gliomas. These radiomics approaches lay the foundation for detecting ATRX status noninvasively.

In this study, we extracted a large number of radiomics features from preoperative MR imaging of low and high-grade gliomas with known ATRX status in this work. We hypothesized that a radiomic signature based on multiparameter MR images to predict ATRX status in patients with low and high-grade gliomas.

## 2. Material and Methods

### 2.1. Study population

This study was approved and reviewed by the institutional review board of the institution (The Second Hospital, Cheeloo College of Medicine, Shandong University). The requirement for informed consent was waived because we used noninvasive methods and data from a previous cohort study. In this retrospective study, we reviewed the clinical records and MR images of glioma patients who underwent surgical treatment at the Second Hospital, Cheeloo College of Medicine, Shandong University between January 2016 and July 2020. The patients were randomly assigned to training or validation set at a ratio of 4:1. All patients in both groups met the following inclusion criteria: (a) pathologically confirmed grade II, III, or IV glioma based on the 2016 World Health Organization classification (3); (b) receiving no systemic treatment, biopsy, or surgery before MRI scan; (c) availability of preoperative T1WI, T2WI, T2FLAIR, contrast-enhanced T1WI (CE-T1WI) and apparent diffusion coefficient (ADC) images; (d) availability of ATRX mutation status (detected by immunohistochemistry [IHC] at our hospital); and (e) availability of clinical characteristics. The exclusion criteria were as follows: (1) unsatisfactory image quality with susceptibility or motion artifacts; and (2) no ATRX information. A flowchart of the inclusion and exclusion criteria is shown in Figure 1.

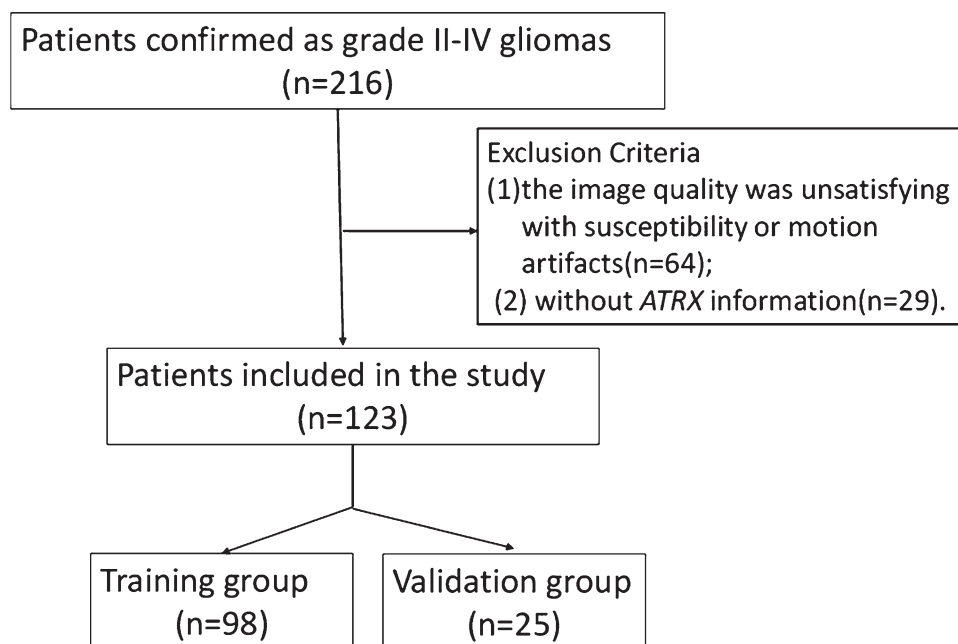


Figure 1. Flowchart depicting the patients enrollment process.

## 2.2. MRI data acquisition

MRI images were acquired using a 3.0 T MR system (Discovery 750; GE Healthcare, Milwaukee, WI, USA) with an 8-channel head coil (GE Medical Systems). Conventional MRI and contrast-enhanced MRI were implemented during the examination. MRI sequence included T1WI, T2WI, T2FLAIR, diffusion weighted imaging (DWI), and CE-T1WI. T2WI was obtained with repetition time/echo time (TR/TE) = 4841/101 ms; field of view (FOV) = 24 × 24 cm; matrix = 192 × 192; number of excitations (NEX) = 1.5; T1WI and CE-T1WI were obtained with inversion time TI/TR/TE/ = 760/1750/24/ms, FOV = 24 × 24 cm, matrix = 320 × 320, NEX = 1. CE-T1WI was performed 2 minutes after intravenous administration of contrast agents (Magnevist, 0.1 mmol/kg, Bayer HealthCare Pharmaceuticals, Wayne, NJ). DWI was performed using the following parameters: TR/TE = 4880/78.6 ms; diffusion gradient encoding, b = 0 and 1000 seconds/mm<sup>2</sup>; FOV = 24 × 24 cm; matrix = 288 × 128; acquisition time = 39 seconds. T2FLAIR images were obtained with TR/TE = 9000/88 ms, FOV = 24 × 24 cm, matrix = 320 × 320, NEX = 1. These images were obtained with an identical section thickness of 5 mm and section space of 1.5 mm.

## 2.3. Tumor segmentation and intensity normalization

The volume of interest (VOI) was manually segmented for all slices on the T1WI, T2WI, T2FLAIR, CE-T1WI, and ADC images based on a radiomics analysis platform (Radcloud, Huiying Medical Technology Co. Ltd.) by 2 experienced radiologists (with 12 years and 16 years of experience in neuro-oncology imaging, respectively). Two neuroradiologists were blinded to the clinical data. A third senior neuroradiologist (with >20 years of experience) made the final decision if the VOI borders were controversial. The regions of interest, including the tumor, possible edema, cystic degeneration and necrosis, were acquired for each patient.

In the imaging and storage of medical images, in order to make the intensity information consistent, the following formula is used to normalize the intensity of MRI images:

$$f(x) = \frac{s(x - \mu_x)}{\sigma_x}$$

where  $f(x)$  is the normalized intensity,  $x$  is the original intensity,  $\mu$  and  $\sigma$  are the mean value and variance, respectively.  $s$  represents an optional scaling whose default is 1.<sup>[28]</sup>

## 2.4. Radiomics feature extraction

In this study, radiomics features were extracted from the platform using the “Pyradiomics” package in Python (version 2.1.2, <https://pyradiomics.readthedocs.io/>). These features can be classified into 4 groups. Group 1 first-order features quantitatively describe the distribution of signal intensity of MR images; Group 2 shape properties, which reflect the 3-dimensional properties of the VOI's shape and size; Group 3 texture features, which could quantify regional heterogeneity differences; Group 4 higher-order statistical features, including the first-order statistics and texture properties after transformation of the original images (using directional low-pass and high-pass filtering, the original feature was decomposed into 8 decompositions).

To guarantee the robustness of the above features, an intra-class correlation coefficient (ICC) cutoff was set for test-retest analysis. ICC >0.80 was considered as evidence of good agreement, and the delineation was repeatedly identified and drawn by the 2 radiologists until the ICC met the requirement.<sup>[29-31]</sup> An example of the manual segmentation process is shown in Figure 2

## 2.5. Feature selection and classification

Because a large number of high-dimensional image features were extracted in the current study, we performed a feature dimension reduction process to select the most valuable features for constructing a radiomics signature. To reduce the redundant features, First, we selected 2267 features from 7045 features using a variance threshold method (variance threshold = 0.8). We then used the Select K best method to further select radiomics features. Finally, 15 optimal features were selected as the radiomics signature using the least absolute shrinkage and selection operator (LASSO) algorithm, as shown in Figure 3.

Subsequently, we utilized a SVM classifier to establish a radiomics-based signature prediction model using data from the training set. Each model was trained using 5-fold cross-validation of

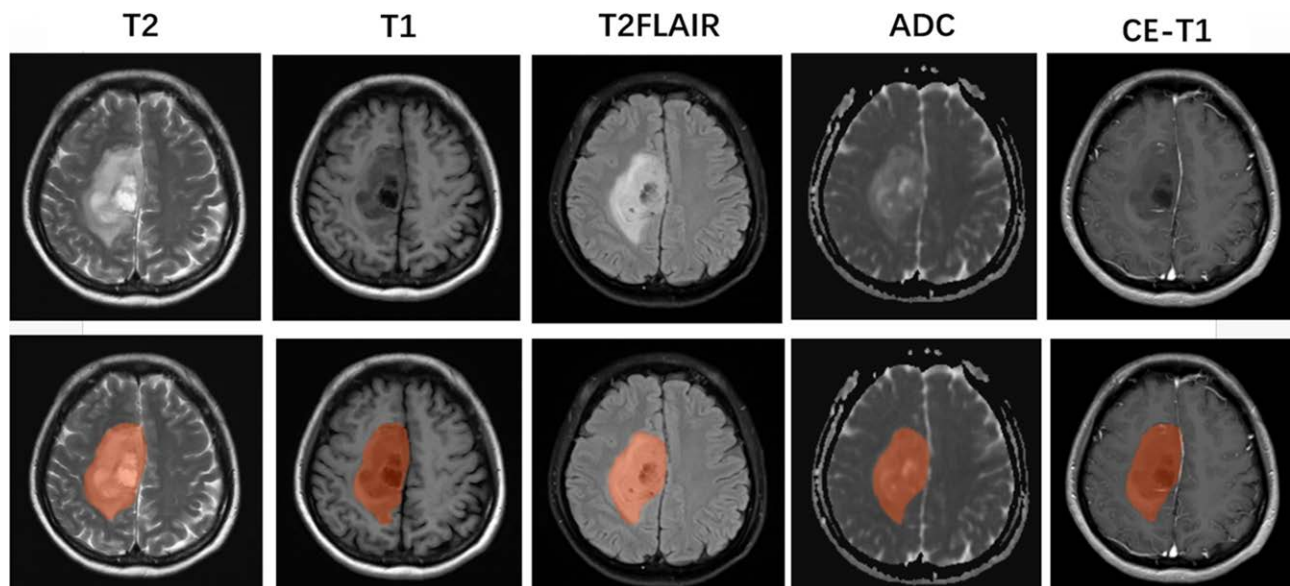


**Figure 2.** Tumor segmentation. After the acquisition of magnetic resonance images, tumor segmentation was conducted using the image data, including T2, T1, T2FLAIR, ADC and CE-T1WI. The orange part in image represents the volume of interest.

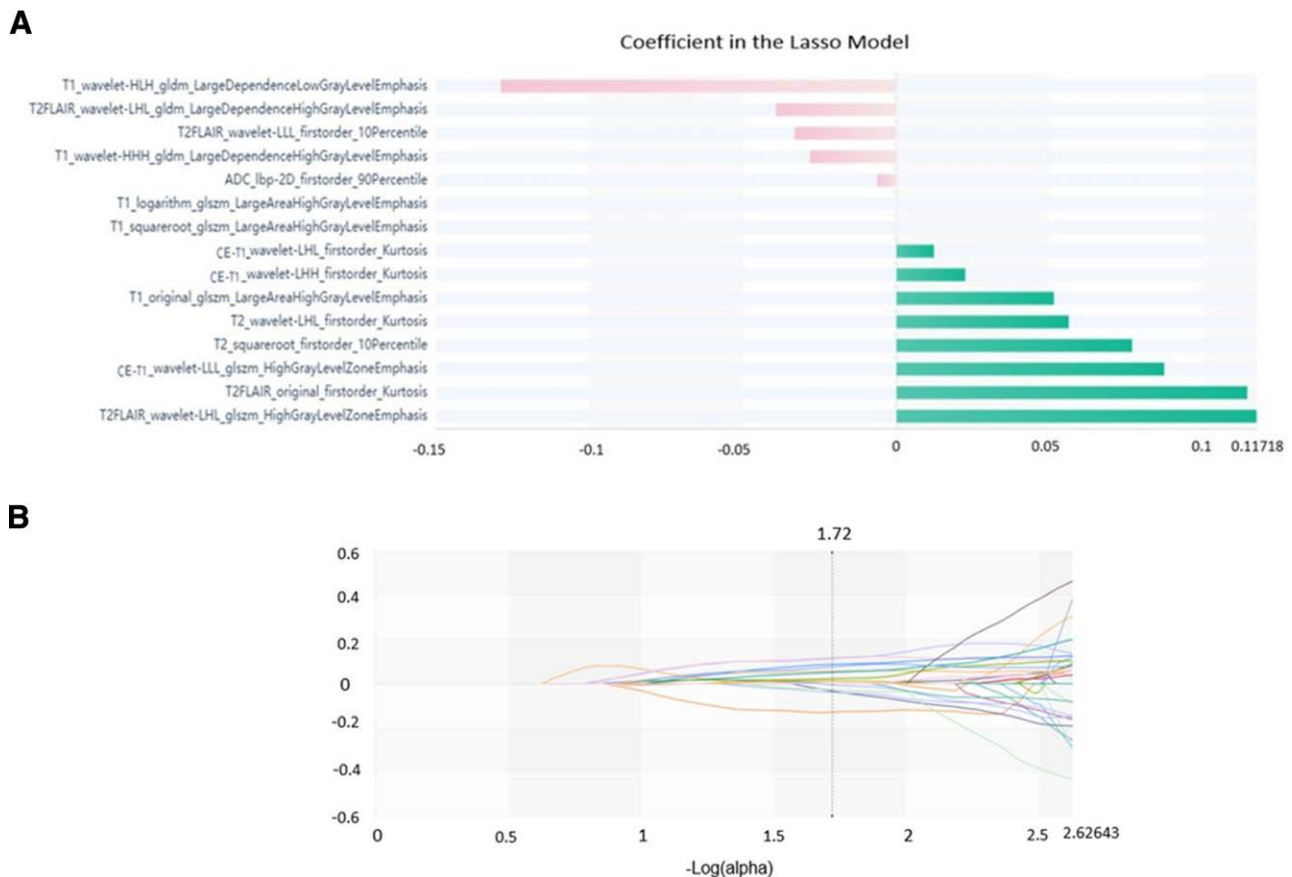


**Figure 3.** The least absolute shrinkage and selection operator algorithm (LASSO) algorithm on feature selection. (A) Distribution and ranking of optimal radiomic features for discriminating between ATRX(-) and ATRX(+) gliomas. (B) Coefficient profiles of the radiomic features in Lasso model. Using Lasso model, fifteen features which are correspond to the optimal tuning parameter ( $\alpha$ ) value were selected.

the training set, and the same model was applied in the validation set. Based on 5-fold cross-validation, the SVM model using the radial basis function (RBF) as the kernel function was used for training, in which the parameters  $C = 1$  and  $\gamma = 0.001$ .

## 2.6. Statistical analysis

The predictive performance of the model was estimated using the area under the curve (AUC) from receiver operating characteristic (ROC) curve analysis in both the training and validation sets. The values of accuracy, sensitivity, and specificity values were calculated.

The chi-square test and Fisher exact test were performed using SPSS Statistics (Version 25.0; IBM, Armonk, NY) to determine the significance of differences in age, sex, histologic grade and type, and tumor location between the ATRX(-) and ATRX(+) groups. The level of confidence was maintained at 95%, a value of  $P < .05$  was considered statistically significant.

## 2.7. Determination of ATRX status

All analyses of ATRX status were performed using IHC by the department of pathology of our institution. Nuclear ATRX-loss was scored as ATRX mutation if tumor cell nuclei were unstained, whereas non-neoplastic cell nuclei, microglial cells, lymphocytes, and astrocytes were strongly positive according to reference criteria.<sup>[32]</sup> A threshold of 10% of strongly positive tumor nuclei was used to assign ATRX expression.<sup>[33]</sup> The IHC interpretation was performed by 2 certified neuropathologists in all cases.

## 3. Results

### 3.1. Clinical characteristics

There were 98 patients (53 males and 45 females) in the training group and 25 patients (15 males and 10 females) in the validation group. The median age of the patients was 43.0 years in the training set and 42.5 years in the validation set, respectively. Among patients enrolled in this study, ATRX(-) was detected in 30.6% (30/98) of patients in training group and 36.0% (9/25) in the validation group. There were significant differences in histological type and tumor location between ATRX(-) and ATRX(+) ( $P < .05$ ). However, no significant differences were found in age, sex, and grade between the 2 datasets ( $P > .05$ ). The statistical results for the patients' clinical characteristics are summarized in Table 1.

### 3.2. Feature selection and the radiomic signature building

A total of 1409 features were extracted from each series, including 19 first-order features, 26 shape features, 75 texture features, and 1289 wavelet features. Thus, amount to 7045 imaging features were obtained from the T1WI, T2WI, FLAIR, CE-T1WI, and ADC images for each patient.

Fifteen radiomic features were selected to generate an ATRX-related radiomic signature using the LASSO logistic regression model, including 5 features derived from T1WI, 2 features derived from T2WI, 4 features derived from T2FLAIR, 3 features derived from CE-T1WI, and 1 features derived from ADC images. A detailed description of the 15 selected features is presented in Table 2.

**Table 1**  
**Associations between ATRX mutation presence and clinical characteristics.**

Clinical characteristics	Subgroup	ATRX(+)	ATRX(-)	P-value
Age(years; mean)	<40 years old	27	16	.336*
	≥40 years old	57	23	
Gender	Male	45	23	.575*
	Female	39	16	
Grade	II	31	13	.625*
	III	19	12	
	IV	34	14	
Histological type	Anaplastic astrocytoma	8	12	.006†
	Anaplastic pleomorphic yellow astrocytoma	5	0	
	Diffuse astrocytoma	13	7	
	Oligodendrocytoma	6	0	
	Oligodendroglioma	10	0	
	Anaplastic oligodendroglioma	12	7	
	Glioblastoma	30	13	
Tumor location	Frontal lobe	23	14	.042†
	Temporal lobe	14	1	
	Parietal lobe	12	7	
	Occipital lobe	7	0	
	Cerebellum	0	1	
	Brainstem	1	0	
	Thalamus	1	1	
	Two or more	26	15	

\*Chi-square test P-value.

†Fisher exact test P-value.

**Table 2**  
**Fifteen features used to predict ATRX mutation in gliomas.**

Radiomic feature	Description	Radiomic class	Filter
LargeDependenceLowGrayLevelEmphasis	Measures the joint distribution of large dependence with lower gray-level values.	gldm	T1_wavelet-HLH
LargeDependenceHighGrayLevelEmphasis	Measures the joint distribution of large dependence with higher gray-level values.	gldm	T2FLAIR_wavelet-LHL
10Percentile	A set of data containing n values is arranged in numerical order from smallest to largest, and the value in the 10% position is called the 10 percentile	firstorder	T2FLAIR_wavelet-LLL
LargeDependenceLowGrayLevelEmphasis	An individual feature can be enabled by submitting the feature name as defined in the unique part of the function signature	gldm	T1_wavelet-HHH
90Percentile	A set of data containing n values is arranged in numerical order from smallest to largest, and the value in the 90% position is called the 90 percentile	firstorder	ADC_lbp-2D
LargeAreaHighGrayLevelEmphasis	Measures the proportion in the image of the joint distribution of larger size zones with higher gray-level values.	glszm	T1_logarithm
LargeAreaHighGrayLevelEmphasis	Measures the proportion in the image of the joint distribution of larger size zones with higher gray-level values.	glszm	T1_squareroot
Kurtosis	Measure of the "peakedness" of the distribution of values in the image ROI.	firstorder	CE-T1_wavelet-LHL
Kurtosis	Measure of the "peakedness" of the distribution of values in the image ROI.	firstorder	CE-T1_wavelet-LHH
LargeAreaHighGrayLevelEmphasis	Measures the proportion in the image of the joint distribution of larger size zones with higher gray-level values	glszm	T1_original
Kurtosis	Measure of the "peakedness" of the distribution of values in the image ROI.	firstorder	T2_wavelet-LHL
10Percentile	A set of data containing n values is arranged in numerical order from smallest to largest, and the value in the 10% position is called the 10 percentile	firstorder	T2_squareroot
HighGrayLevelZoneEmphasis	Measures the distribution of the higher gray-level values, with a higher value indicating a greater proportion of higher gray-level values and size zones in the image.	glszm	CE-T1_wavelet-LLL
Kurtosis	Measure of the "peakedness" of the distribution of values in the image ROI.	firstorder	T2FLAIR_original
HighGrayLevelZoneEmphasis	Measures the distribution of the higher gray-level values, with a higher value indicating a greater proportion of higher gray-level values and size zones in the image.	glszm	T2FLAIR_wavelet-LHL

GLDM = gray-level dependence matrix, GLSZM = gray-level size zone matrix.

### 3.3. ATRX genotype prediction

As shown in Table 3, in the training set, the AUC was 0.93 (95% confidence interval [CI]: 0.87–1.0), sensitivity was 0.91, and specificity was 0.82 with a prediction accuracy of 0.88. In the validation set, the AUC was 0.84 (95% CI: 0.63–0.91), sensitivity was 0.73, and specificity was 0.86 with an accuracy of 0.79. The ROC curves for the 2 models are shown in Figure 4.

### 4. Discussion

Conventional and contrast-enhanced MRI are common imaging modalities for glioma preoperatively. In the current study, we used MR multiparameter imaging for radiomics analysis. To the best of our knowledge, this is the first time to study ATRX status in gliomas using MR multiparameter radiomics features. The model established in our study performed effectively in both the training group and the validation group, affirming the

**Table 3**  
**Performances of the classifiers with radiomics signature.**

	Training set				Validation set			
	AUC	95% CI	Se	Sp	AUC	95% CI	Se	Sp
ATRX(-)	0.93	0.87–1.0	0.91	0.82	0.84	0.63-0.91	0.73	0.86
ATRX(+)	0.93	0.87–1.0	0.82	0.91	0.84	0.63-0.91	0.86	0.73

AUC = area under the receiver operating characteristics curve, CIs = confidence intervals, Se = sensitivity, Sp = specificity.

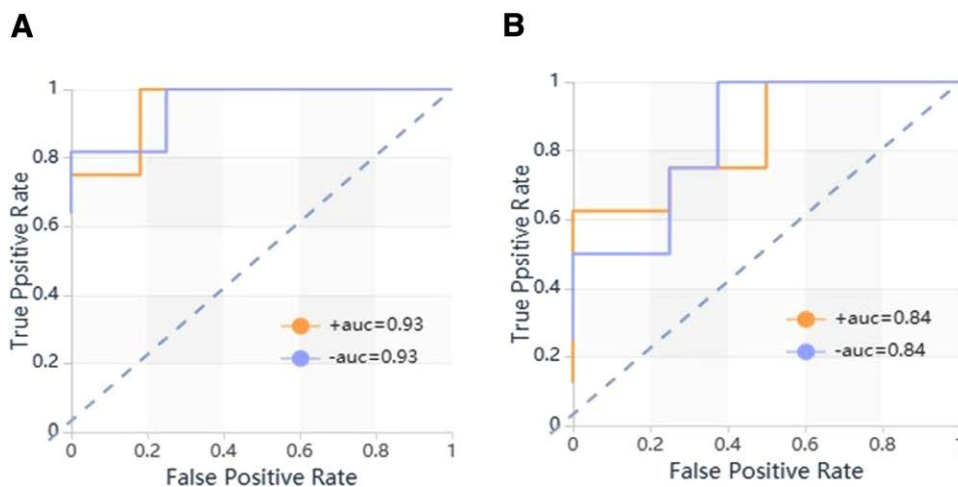


**Figure 4.** Receiver operating characteristic (ROC) curves for ATRX genotype prediction in training and validation sets. (A) In the training set, the area under the curve (AUC) was 0.93. (B) In the validation set, the AUC was 0.84.

hypothesis that radiomics can predict ATRX mutation status in gliomas. The AUC of 0.93 and 0.84 in the training and validation sets respectively, are comparable to results from other studies that have used MRI T2WI only.<sup>[34]</sup> To establish the radiomics model, the LASSO algorithm was applied to select a subset of 15 features from the 7045 extracted radiomic features. The LASSO regression is characterized by variable selection and regularization while fitting the generalized linear model that is widely used in radiomics analysis. The SVM classifier is an effective tool that exhibits better performance than other algorithms with regard to pattern recognition.<sup>[35–37]</sup> In the present study, the LASSO algorithm was used in combination with the SVM classifier to develop a method capable of effectively predicting ATRX mutation status in gliomas. Ren et al<sup>[38]</sup> revealed that low-grade gliomas with ATRX(-) may be associated with higher levels of difference variance and standard deviation, but lower entropy, which could be used to identify the status of ATRX (-) from ATRX(+) in low-grade gliomas. These results suggest that highly accurate and reliable classification models can promote the success of radiomics in precision oncology.

We analyzed clinical data including age, sex, histological grade and type, and tumor location in this study. We found that there were significant differences in histological type and tumor location between the ATRX(-) and ATRX(+) groups. The contribution of information on tumor location in differentiating between molecular genetic subsets has been tested in a few recent studies. Ikemura et al<sup>[39]</sup> conducted an immunohistochemical analysis and demonstrated that ATRX-loss glioblastomas occurred more frequently in non-hemispheric locations and affected younger patients. However, there were no significant differences in age between the ATRX(-) and ATRX(+) groups in our study. Further confirmation is needed because of our relatively small number of cases (25 grade II/III cases in the ATRX(-) group).

ATRX has been shown to be a potential biomarker and mainly implicated in the chromatin silencing processes. ATRX

mutations or loss, is associated with a decrease in mRNA expression,<sup>[40]</sup> accompanied by an alternative lengthening of telomeres (ALT) phenotype. These behaviors can affect the biological behaviors of astrocytic tumor cells by inducing an increase in apoptotic cells and reducing proliferation in glioma cells, which is associated with favorable survival of patients with astrocytic tumors.<sup>[41,42]</sup> Flynn et al<sup>[43]</sup> indicated that the protein kinase ATR inhibitors may be useful in the treatment of ALT-positive cancers. Another study reported that ATRX inhibitors can disrupt ALT and induce chromosome fragmentation and cell death.<sup>[44]</sup> In this sense, ATRX-loss cells could be targeted by epigenetic therapies aiming to restore normal chromatin silencing levels. On the other hand, ATRX-loss cells may be particularly vulnerable to polymerase-1 inhibition, providing a potential therapeutic approach to treat these cells.<sup>[45]</sup> However, this approach has not been evaluated in cancer cells.

ATRX mutations can provide useful information on glioma prognosis. Among tumors with isocitrate dehydrogenase (IDH) mutations and no loss of chromosome 1p/19q, the loss of ATRX is associated with improved progression-free and overall survival.<sup>[33,46]</sup> Studies on in regard to adult anaplastic gliomas have shown that ATRX mutations identify a subgroup of IDH mutant astrocytic tumors with better prognosis.<sup>[40]</sup> Olar et al<sup>[47]</sup> found adult gliomas with ATRX mutations in wild-type IDH1 adult gliomas had higher survival rates. Additionally, recent studies have confirmed that ATRX-mutated glioblastomas have a survival advantage.<sup>[1,48]</sup> Based on these observations, ATRX may serve as a novel and valuable therapeutic target in clinical practice.

In the era of big data, radiomics has become a robust tool for medical image analysis, which can help solve important clinical questions and provide the necessary information for patient-specific personalized treatments (i.e., precision medicine). Advanced radiomics analytic tools for quantitative analysis of biomarkers with the goal of refining clinical decision making and improving

patient outcomes can significantly improve our ability to stratify patients for true personalized cancer care.

Although radiomics features performed well, there were some limitations to our study. First, studies with larger datasets from multiple sites are required to validate the initial results. Second, multi-model imaging data (such as diffusion tensor, perfusion imaging, and magnetic resonance spectroscopy and so forth) need to be integrated into our model in the future to improve its performance. Third, other critical biomarkers (such as IDH, P53, Ki67) should be considered in future studies.

## 5. Conclusion

In conclusion, the use of radiomics analysis based on MR multisequence images to identify ATRX status in patients with gliomas was predicted effectively. The proposed noninvasive methodology for genotype detection may aid the neuro-oncologist in more accurately predicting prognosis prior to tissue diagnosis and in personalizing the follow-up and treatment regimen without the need for or prior to invasive tissue sampling.

## Author contributions

Linlin Meng and Guangrui Shao made substantial contributions to the conception and design of the study. Linlin Meng performed the statistical analysis and drafted the manuscript. Ran Zhang reviewed all imaging studies. Liangguo Fa, Lulu Zhang, and Linin Wang contributed to the conception of the work and substantively revised it. All authors agreed to participate and approved the submitted version.

## References

- [1] Suzuki H, Aoki K, Chiba K, et al. Mutational landscape and clonal architecture in grade II and III gliomas. *Nat Genet.* 2015;47:458–68.
- [2] Louis DN, Perry A, Burger P, et al. International society of neuropathology–haarlem consensus guidelines for nervous system tumor classification and grading. *Brain Pathol.* 2014;24:429–35.
- [3] Sonoda Y, Yokoo H, Tanaka S, et al. Practical procedures for the integrated diagnosis of astrocytic and oligodendroglial tumors. *Brain Tumor Pathol.* 2019;36:56–62.
- [4] Louis DN, Perry A, Reifenberger G, et al. The 2016 world health organization classification of tumors of the central nervous system: a summary. *Acta Neuropathol.* 2016;131:803–20.
- [5] Synhaeve NE, Van Den Bent MJ, French PJ, et al. Clinical evaluation of a dedicated next generation sequencing panel for routine glioma diagnostics. *Acta Neuropathol Commun.* 2018;6:126.
- [6] Pekmezci M, Rice T, Molinaro AM, et al. Adult infiltrating gliomas with WHO 2016 integrated diagnosis: additional prognostic roles of ATRX and TERT. *Acta Neuropathol.* 2017;133:1001–16.
- [7] Van Den Bent MJ, Weller M, Wen PY, et al. A clinical perspective on the 2016 WHO brain tumor classification and routine molecular diagnostics. *Neuro Oncol.* 2017;19:614–24.
- [8] Núñez FJ, Mendez FM, Kadiyala P, et al. IDH1-R132H acts as a tumor suppressor in glioma via epigenetic up-regulation of the DNA damage response. *Sci Transl Med.* 2019;11:eaq1427.
- [9] Gibbons RJ, Wada T, Fisher CA, et al. Mutations in the chromatin-associated protein ATRX. *Hum Mutat.* 2008;29:796–802.
- [10] Bassett AR, Cooper SE, Ragab A, et al. The chromatin remodeling factor dATRX is involved in heterochromatin formation. *PLoS One.* 2008;3:e2099.
- [11] Eckel-Passow JE, Lachance DH, Molinaro AM, et al. Glioma groups based on 1p/19q, IDH, and TERT promoter mutations in tumors. *N Engl J Med.* 2015;372:2499–508.
- [12] Gao J, Aksoy BA, Dogrusoz U, et al. Integrative analysis of complex cancer genomics and clinical profiles using the cBioPortal. *Sci Signal.* 2013;6:pl1.
- [13] Gibbons RJ, Pellagatti A, Garrick D, et al. Identification of acquired somatic mutations in the gene encoding chromatin-remodeling factor ATRX in the alpha-thalassemia myelodysplasia syndrome (ATMDS). *Nat Genet.* 2003;34:446–9.
- [14] Jiao Y, Killela PJ, Reitman ZJ, et al. Frequent ATRX, CIC, FUBP1 and IDH1 mutations refine the classification of malignant gliomas. *Oncotarget.* 2012;3:709–22.
- [15] Kannan K, Inagaki A, Silber J, et al. Whole-exome sequencing identifies ATRX mutation as a key molecular determinant in lower-grade glioma. *Oncotarget.* 2012;3:1194–203.
- [16] Liu XY, Gerges N, Korshunov A, et al. Frequent ATRX mutations and loss of expression in adult diffuse astrocytic tumors carrying IDH1/IDH2 and TP53 mutations. *Acta Neuropathol.* 2012;124:615–25.
- [17] Brat DJ, Verhaak RG, Aldape KD, et al. Comprehensive, integrative genomic analysis of diffuse lower-grade gliomas. *N Engl J Med.* 2015;372:2481–98.
- [18] Ceccarelli M, Barthel FP, Malta TM, et al. Molecular profiling reveals biologically discrete subsets and pathways of progression in diffuse glioma. *Cell.* 2016;164:550–63.
- [19] Leeper HE, Caron AA, Decker PA, et al. IDH mutation, 1p19q codeletion and ATRX loss in WHO grade II gliomas. *Oncotarget.* 2015;6:30295–305.
- [20] Hu WM, Wang F, Xi SY, et al. Practice of the new integrated molecular diagnostics in gliomas: experiences and new findings in a single Chinese center. *J Cancer.* 2020;11:1371–82.
- [21] Schwartzentruber J, Korshunov A, Liu XY, et al. Driver mutations in histone H3.3 and chromatin remodeling genes in paediatric glioblastoma. *Nature.* 2012;482:226–31.
- [22] Cai JQ, Zhang CB, Zhang W, et al. ATRX, IDH1-R132H and Ki-67 immunohistochemistry as a classification scheme for astrocytic tumors. *Oncoscience.* 2016;3:258–65.
- [23] Modrek AS, Golub D, Khan T, et al. Low-grade astrocytoma mutations in IDH1, P53, and ATRX cooperate to block differentiation of human neural stem cells via repression of SOX2. *Cell Rep.* 2017;21:1267–80.
- [24] Altan A, Karasu S. Recognition of COVID-19 disease from X-ray images by hybrid model consisting of 2D curvelet transform, chaotic salp swarm algorithm and deep learning technique. *Chaos Solitons Fractals.* 2020;140:110071.
- [25] Zhang B, Chang K, Ramkissoon S, et al. Multimodal MRI features predict isocitrate dehydrogenase genotype in high-grade gliomas. *Neuro Oncol.* 2017;19:109–17.
- [26] Sun Z, Li Y, Wang Y, et al. Radiogenomic analysis of vascular endothelial growth factor in patients with diffuse gliomas. *Cancer Imaging.* 2019;19:68.
- [27] Kickingereder P, Bonekamp D, Nowosielski M, et al. Radiogenomics of glioblastoma: machine learning-based classification of molecular characteristics by using multiparametric and multiregional MR imaging features. *Radiology.* 2016;281:907–18.
- [28] Freedman D, Pisani R, Purves R. *Statistics: fourth international student edition.* New York: W.W. Norton & Company; 2007. ISBN 9780393930436.
- [29] Huang YQ, Liang CH, He L, et al. Development and validation of a radiomics nomogram for preoperative prediction of lymph node metastasis in colorectal cancer. *J Clin Oncol.* 2016;34:2157–64.
- [30] Karimi S, Nourinia R, Mashayekhi A. Circumscribed choroidal hemangioma. *J Ophthalmic Vis Res.* 2015;10:320–28.
- [31] Demirci H, Mashayekhi A, Shields CL, et al. Iris melanocytoma: clinical features and natural course in 47 cases. *Am J Ophthalmol.* 2005;139:468–75.
- [32] Reuss DE, Sahn F, Schimpf D, et al. ATRX and IDH1-R132H immunohistochemistry with subsequent copy number analysis and IDH sequencing as a basis for an “integrated” diagnostic approach for adult astrocytoma, oligodendroglioma and glioblastoma. *Acta Neuropathol.* 2015;129:133–46.
- [33] Wiestler B, Capper D, Holland-Letz T, et al. ATRX loss refines the classification of anaplastic gliomas and identifies a subgroup of IDH mutant astrocytic tumors with better prognosis. *Acta Neuropathol.* 2013;126:443–51.
- [34] Li Y, Liu X, Qian Z, et al. Genotype prediction of ATRX mutation in lower-grade gliomas using an MRI radiomics signature. *Eur Radiol.* 2018;28:2960–8.
- [35] Fu MR, Wang Y, Li C, et al. Machine learning for detection of lymphedema among breast cancer survivors. *Mhealth.* 2018;4:17.
- [36] Zhang G, Piccardi M, Zare Borzeshi E. Sequential labeling with structural SVM under nondecomposable losses. *IEEE Trans Neural Netw Learn Syst.* 2017;29:4177–88.
- [37] Hotzy F, Theodoridou A, Hoff P, et al. Machine learning: an approach in identifying risk factors for coercion compared to binary logistic regression. *Front Psychiatry.* 2018;9:258.
- [38] Ren Y, Zhang X, Rui W, et al. Noninvasive prediction of IDH1 mutation and ATRX expression loss in low-grade gliomas using multiparametric MR radiomic features. *J Magn Reson Imaging.* 2019;49:808–17.

- [39] Ikemura M, Shibahara J, Mukasa A, et al. Utility of ATRX immunohistochemistry in diagnosis of adult diffuse gliomas. *Histopathology*. 2016;69:260–7.
- [40] Xie Y, Tan Y, Yang C, et al. Omics-based integrated analysis identified ATRX as a biomarker associated with glioma diagnosis and prognosis. *Cancer Biol Med*. 2019;16:784–96.
- [41] Napier CE, Huschtscha LI, Harvey A, et al. ATRX represses alternative lengthening of telomeres. *Oncotarget*. 2015;6:16543–58.
- [42] Cai J, Chen J, Zhang W, et al. Loss of ATRX, associated with DNA methylation pattern of chromosome end, impacted biological behaviors of astrocytic tumors. *Oncotarget*. 2015;6:18105–15.
- [43] Flynn RL, Cox KE, Jeitany M, et al. Alternative lengthening of telomeres renders cancer cells hypersensitive to ATR inhibitors. *Science*. 2015;347:273–7.
- [44] Bush NA, Butowski N. The effect of molecular diagnostics on the treatment of glioma. *Curr Oncol Rep*. 2017;19:26.
- [45] Haase S, Garcia-Fabiani MB, Carney S, et al. Mutant ATRX: uncovering a new therapeutic target for glioma. *Expert Opin Ther Targets*. 2018;22:599–613.
- [46] Cai J, Zhu P, Zhang C, et al. Detection of ATRX and IDH1-R132H immunohistochemistry in the progression of 211 paired gliomas. *Oncotarget*. 2016;7:16384–95.
- [47] Olar A, Sulman EP. Molecular markers in low-grade glioma—toward tumor reclassification. *Semin Radiat Oncol*. 2015;25:155–63.
- [48] Koschmann C, Calinescu AA, Nunez FJ, et al. ATRX loss promotes tumor growth and impairs nonhomologous end joining DNA repair in glioma. *Sci Transl Med*. 2016;8:328ra–28.